Molecular Therapy
Original Article

Targeting RNA oxidation by ISG20-mediated degradation is a potential therapeutic strategy for acute kidney injury

Meng Jia,[1] Liang Li,[1] Ruiqi Chen,[1] Junyao Du,[1] Zhe Qiao,[1] Di Zhou,[1] Min Liu,[1] Xiaojie Wang,[1] Jichao Wu,[1] Yusheng Xie,[1] Yu Sun,[1] Yan Zhang,[1] Ziying Wang,[1] Tao Zhang,[2] Huili Hu,[3] Jinpeng Sun,[4] Wei Tang,[5] and Fan Yi[1,6]

[1]Department of Pharmacology, School of Basic Medical Sciences, Shandong University, Jinan 250012, China; [2]Department of Biostatistics, School of Public Health, Shandong University, Jinan 250012, China; [3]Department of Systems Biomedicine and Research Center of Stem Cell and Regenerative Medicine, School of Basic Medical Sciences, Shandong University, Jinan 250012, China; [4]Department of Biochemistry and Molecular Biology, School of Basic Medical Sciences, Shandong University, Jinan 250012, China; [5]Department of Pathogenic Biology, School of Basic Medical Sciences, Shandong University, Jinan 250012, China; [6]The Key Laboratory of Cardiovascular Remodeling and Function Research, Chinese Ministry of Education, Cheeloo College of Medicine, Shandong University, Jinan 250012, China

Oxidative stress plays a central role in the pathophysiology of acute kidney injury (AKI). Although RNA is one of the most vulnerable cell components to oxidative damage, it is unclear whether RNA oxidation is involved in the pathogenesis of AKI. In this study, we found that the level of RNA oxidation was significantly enhanced in kidneys of patients with acute tubular necrosis (ATN) and in the renal tubular epithelial cells (TECs) of mice with AKI, and oxidized RNA overload resulted in TEC injury. We further identified interferon-stimulated gene 20 (ISG20) as a novel regulator of RNA oxidation in AKI. Tubule-specific deficiency of ISG20 significantly aggravated renal injury and RNA oxidation in the ischemia/reperfusion-induced AKI mouse model and ISG20 restricted RNA oxidation in an exoribonuclease activity-dependent manner. Importantly, overexpression of ISG20 protected against oxidized RNA overproduction and renal ischemia/reperfusion injury in mice and ameliorated subsequent protein aggresome accumulation, endoplasmic reticulum stress, and unfolded protein response. Thus, our findings provide direct evidence that RNA oxidation contributes to the pathogenesis of AKI and that ISG20 importantly participates in the degradation of oxidized RNA, suggesting that targeting ISG20-handled RNA oxidation may be an innovative therapeutic strategy for AKI.

INTRODUCTION

Excessive reactive oxygen species (ROS) can induce oxidative stress, leading to DNA, RNA, lipid, and protein oxidative damage and ultimately cell death.[1,2] Oxidative stress represents a central aggravating factor in the initiation and progression of acute kidney injury (AKI), making it a possible target for therapies.[3] However, challenges remain for the clinical translation of antioxidants in AKI owing to potential adverse effects.[1] More studies are needed to develop new therapies that can address oxidative damage in AKI.

RNA is more vulnerable to oxidation than other cellular components.[4] Emerging evidence indicates that RNA oxidation is linked to a range of diseases and pathological conditions, such as neurodegenerative diseases, diabetes, heart failure, hemochromatosis, and β cell destruction.[5,6] In patients with Alzheimer's disease, Parkinson's disease, amyotrophic lateral sclerosis, and Huntington's disease, RNA is highly oxidized in the early stage of the disease preceding cell death.[7] High urinary excretion of 8-hydroxyguanosine (8-OHG), the most abundant oxidized base in oxidized RNA and a marker of RNA oxidation, is highly predictive of death in newly diagnosed type 2 diabetics.[8,9] In kidney disease, high levels of oxidized RNA were found in the plasma and urine of patients with chronic kidney disease (CKD),[10] and RNA oxidation was also detected to be more apparent than DNA oxidation in the early stage of diabetic nephropathy in *db/db* mice.[11] ROS are the main cause of RNA oxidative damage, which are generated through the Fenton reaction and are promoted by mitochondrial dysfunction.[5] Increased levels of ROS and oxidative stress in AKI may contribute to the production of RNA oxidation. However, it is still unclear whether RNA oxidation is involved in the pathogenesis of AKI. Importantly, the mechanisms of how cells handle oxidized RNA have not been identified in the kidney so far. Therefore, identifying the contribution of RNA oxidation to AKI and the key regulators of RNA oxidation in kidney injuries may provide clues to develop new therapeutic strategies for patients with kidney disease.

Degradation is believed to play a major role in eliminating oxidized RNA.[7,12] RNAs are generally degraded by exoribonucleolytic

Received 17 April 2023; accepted 10 July 2023;
https://doi.org/10.1016/j.ymthe.2023.07.008.

Correspondence: Wei Tang, Department of Pathogenic Biology, School of Basic Medical Sciences, Shandong University, Jinan 250012, China.
E-mail: weitang@sdu.edu.cn
Correspondence: Fan Yi, Department of Pharmacology, School of Basic Medical Sciences, Shandong University, Jinan 250012, China.
E-mail: fanyi@sdu.edu.cn

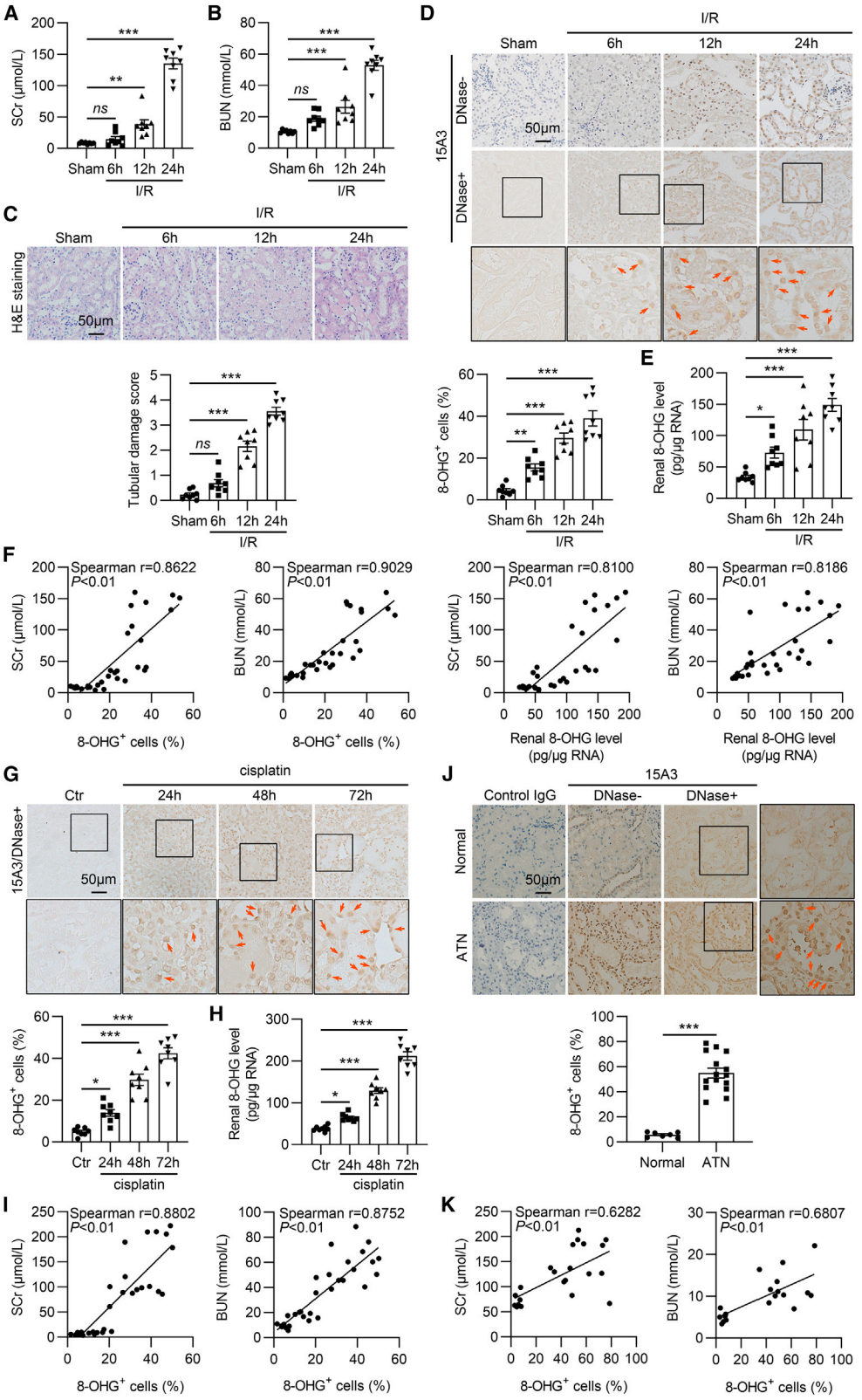

(legend on next page)

reactions in the 5′-3′ or 3′-5′ directions catalyzed by 5′-3′ or 3′-5′ exoribonucleases,[13] and 3′-5′ exoribonucleases are key enzymes in the degradation of superfluous or aberrant RNAs.[14] Nuclear 3′-5′ exoribonuclease interferon-stimulated gene 20 (ISG20), also known as human estrogen-regulated transcript 45 protein (HEM45), belongs to the DEDDh subgroup of the death effector domain containing (DEDD) exonuclease superfamily, and exerts a strong substrate preference of single-stranded RNA (ssRNA) over single-stranded DNA.[15] This study demonstrates for the first time that early elevated RNA oxidation functionally contributes to renal tubular epithelial cell (TEC) injury in AKI and that overexpression of ISG20 protects against renal ischemia/reperfusion injury (IRI) by mediating the degradation of oxidized RNA, thereby preventing the activation of endoplasmic reticulum (ER) stress and unfolded protein response (UPR) cascades. A better understanding of the pathological function of RNA oxidation and the underlying handling mechanisms will provide unexpected opportunities for developing new therapies for various oxidative stress-related diseases.

RESULTS

RNA oxidation was markedly induced in the kidneys of mice with AKI

To determine the oxidized RNA levels in the kidney under AKI conditions, a renal IRI mouse model was constructed and confirmed by increased serum creatinine (SCr) and blood urea nitrogen (BUN) levels (Figures 1A and 1B) and renal morphological injury (Figure 1C). Then, oxidized RNA levels in the kidney were determined by immunohistochemical staining using the DNA/RNA damage monoclonal antibody [15A3], which recognizes the oxidized nucleosides 8-OHG in RNA and 8-hydroxy-2′-deoxyguanosine (8-OHdG) in DNA. To visualize the specific staining of 8-OHG, the recognition of 8-OHdG in DNA by 15A3 antibody should be avoided. Therefore, the kidney sections were pretreated with DNase I to digest DNA before incubation with antibody. As shown in Figure 1D, the intensity of the 15A3 signal, primarily located in the nuclei of renal TECs, was increased in DNase-treated kidney sections from IRI mice at the early stage of renal IRI (6 h after reperfusion), when there was no statistical renal injury or renal function decline. Oxidized RNA levels were further increased at 12 and 24 h after reperfusion, indicating an enhanced RNA oxidation status in the kidneys of IRI mice, which was further confirmed by enzyme-linked immunosorbent assay (ELISA) of renal RNA extracts (Figure 1E). Importantly, the renal 8-OHG-positive cell percentage and renal 8-OHG levels were positively correlated with the SCr and BUN levels in the renal IRI mouse model (Figure 1F). Enhanced RNA oxidation and a positive correlation between renal RNA oxidation and AKI severity were also found in mice with cisplatin-induced AKI (Figures 1G–1I and S1). Furthermore, compared with kidney tissues obtained from patients who underwent tumor nephrectomies without other renal diseases (normal, n = 7), RNA oxidation was significantly elevated in the kidneys of patients with biopsy-proven acute tubular necrosis (ATN) (n = 15) (Figure 1J), a common type of clinical AKI. The percentage of renal 8-OHG-positive cells was positively correlated with the SCr and BUN levels of all subjects (Figure 1K).

RNA oxidation overload led to renal TEC injury

Renal proximal TECs play a central role in renal physiology and are particularly sensitive to ischemia and xenobiotic nephrotoxicity compared with other cell types in the kidney. In addition, considering the major distribution of enhanced oxidized RNA in renal TECs in AKI, human proximal TECs (HK-2) were used for the *in vitro* analysis in this study. Consistent with *in vivo* data, increased oxidized RNA levels in HK-2 cells exposed to hypoxia/reoxygenation (H/R) compared with the control cells were observed by RNA dot blot assay (Figure 2A). Immunocytochemistry analysis and immunofluorescence staining confirmed this finding and demonstrated that the oxidized RNA was mainly located in the nucleus (Figures 2B and 2C). We next evaluated the cytotoxic effect of oxidative RNA on renal TECs *in vitro*. HK-2 cells were subjected to hypotonic treatment with oxidized RNA produced by the Fenton reaction (Figure 2D) and the elevated intracellular RNA oxidation was confirmed by RNA dot blot analysis (Figure 2E). Compared with normal RNA hypotonic treatment, oxidized RNA hypotonic treatment resulted in enhanced percentage of dead and apoptotic HK-2 cells (Figures 2F and 2G).

3′-5′-Exoribonuclease ISG20 was upregulated in the kidney with AKI

RNA degradation plays a major role in eliminating oxidized RNA, and exoribonucleases are key enzymes in the degradation of superfluous or aberrant RNA. Therefore, the expression status of exoribonucleases in the kidneys of IRI mice was surveyed by next-generation RNA sequencing. As shown in Figure 3A, the transcriptional

Figure 1. RNA oxidation was significantly upregulated in the kidneys of mice and patients with AKI

(A) Serum creatinine (SCr) levels of mice after renal ischemia/reperfusion (n = 8). (B) Blood urea nitrogen (BUN) levels of mice after renal ischemia/reperfusion (n = 8). (C) Representative photomicrographs of hematoxylin and eosin (H&E) staining and quantitative assessment of tubular damage in kidneys from mice after renal ischemia/reperfusion (n = 8). (D) Representative photomicrographs of 15A3 antibody immunohistochemical staining of kidney sections with or without DNase treatment and quantification of 8-OHG-positive (8-OHG$^+$) cells in kidney sections with DNase treatment to assess RNA oxidation in renal cells (n = 8). Red arrows indicate representative 8-OHG$^+$ cells. (E) Renal 8-OHG levels of mice after renal ischemia/reperfusion (n = 8). (F) Correlation between renal 8-OHG$^+$ cell percentage, renal 8-OHG levels, and SCr and BUN levels in the renal IRI mouse model. (G) Representative photomicrographs of 15A3 antibody immunohistochemical staining of kidney sections with DNase treatment and quantification of 8-OHG$^+$ cells in kidneys from mice after cisplatin treatment (n = 8). Red arrows indicate representative 8-OHG$^+$ cells. (H) Renal 8-OHG levels of mice after cisplatin treatment (n = 8). (I) Correlation between renal 8-OHG$^+$ cell percentage and SCr and BUN levels in the cisplatin-induced AKI mouse model. (J) Representative photomicrographs of 15A3 antibody immunohistochemical staining of kidney sections with or without DNase treatment and quantification of 8-OHG$^+$ cells in kidney sections of normal subjects (n = 7) and patients with acute tubular necrosis (ATN) (n = 15). Human kidneys stained with normal IgG in place of the corresponding primary antibodies were used as negative controls. Red arrows indicate representative 8-OHG$^+$ cells. (K) Correlation between renal 8-OHG$^+$ cell percentage and available SCr and BUN data of normal subjects and ATN patients. Data are represented as the mean ± SEM. *$p < 0.05$, **$p < 0.01$, ***$p < 0.001$; ns, not significant. See also Figure S1.

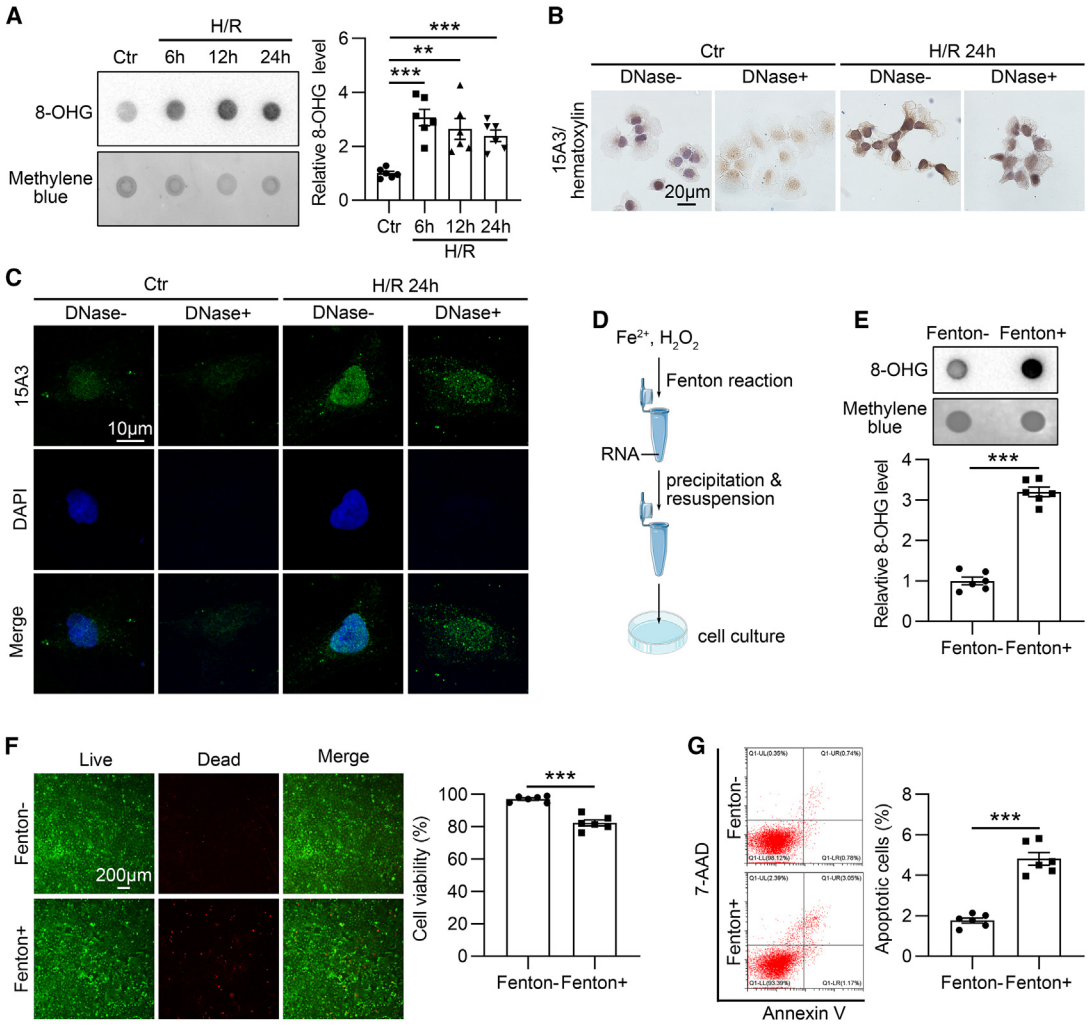

Figure 2. Oxidized RNA overload resulted in renal tubular epithelial cell death

(A) Representative RNA dot blot documents and summarized data showing the relative 8-OHG levels of RNA extracts from HK-2 cells with hypoxia/reoxygenation (H/R) treatment (n = 6). Methylene blue staining validated the equal loading amount of RNA. (B) Representative photomicrographs of 15A3 antibody immunocytochemistry staining of HK-2 cells with H/R treatment. (C) Representative photomicrographs of 15A3 antibody immunofluorescence staining of HK-2 cells with H/R treatment. Nuclei were revealed using 4′,6-diamidino-2-phenylindole (DAPI) staining. (D) A schematic diagram showing the procedure of oxidized RNA treatment of HK-2 cells. (E) Representative RNA dot blot documents and summarized data showing the relative 8-OHG levels of RNA extracts from HK-2 cells with oxidized RNA hypotonic treatment (n = 6). (F) Photomicrographs and quantifications showing the viability of HK-2 cells with oxidized RNA hypotonic treatment (n = 6). The green channel depicts live cells, and the red channel depicts compromised/dead cells. (G) Representative flow cytometry analysis and quantitative data depicting the apoptosis of HK-2 cells with oxidized RNA hypotonic treatment (n = 6). Data are represented as the mean ± SEM. **p < 0.01, ***p < 0.001.

expression of the 3′-5′-exoribonucleases PDE12 and ISG20 was significantly upregulated and ERI2 was downregulated in the kidneys from IRI mice. The downregulated expression of ERI2 and upregulated expression of PDE12 at the mRNA level in the kidneys from IRI mice were confirmed by real-time RT-PCR (Figure 3B), but there was no significant change in their protein levels (Figure 3C). However, both the mRNA and protein levels of ISG20 were significantly increased in the kidneys from IRI mice (Figures 3D and 3E), and the immunohistochemical staining showed that the upregulated ISG20 expression was mainly localized in the nuclei of TECs (Figure 3F). To further define the tubular segment specificity of ISG20 expression in the kidney, double immunostaining for ISG20 (red) and various tubular markers (green) was carried out. The following segment-specific tubular markers were used: lotus tetragonolobus lectin (LTL) for the proximal tubule, calbindin D28K for the distal tubule, and aquaporin-3 for the collecting duct. As shown in Figure S2, the expression of ISG20 was very low in the kidneys from Sham-operated mice, and it was upregulated in the proximal tubules, distal tubules, and collecting ducts of IRI mice. Increased ISG20 mRNA and protein levels were also found in the kidneys of cisplatin-induced

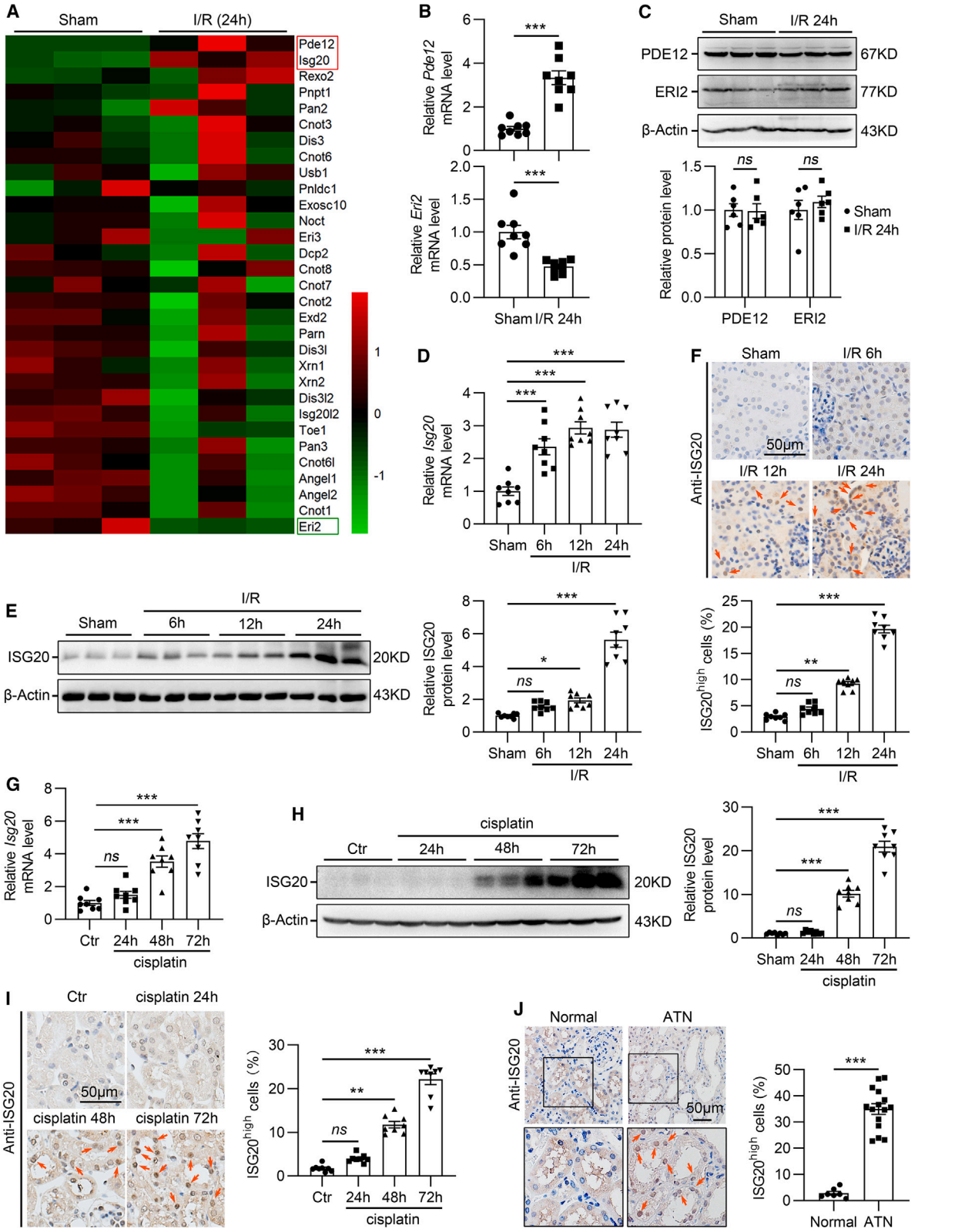

(legend on next page)

AKI model mice (Figures 3G–3I). Moreover, upregulated expression of ISG20 in the kidneys of patients with biopsy-proven ATN was demonstrated by immunohistochemical staining (Figure 3J).

Tubule-specific deficiency of ISG20 exacerbated renal injury in IRI mice

We generated tubule-specific ISG20-deficient ($Cre^{+}/ISG20^{fl/fl}$) mice by a Cre-*loxP* recombination system involving Cdh16-Cre, which was confirmed by tail genotyping (Figure 4A), western blot analysis (Figure 4B), and immunohistochemical staining analysis of kidneys (Figure 4C). Although $Cre^{+}/ISG20^{fl/fl}$ mice were phenotypically normal and had no appreciable defect in renal morphology and function, tubule-specific ISG20 deficiency significantly aggravated renal injuries in IRI mice. The levels of SCr (Figure 4D) and BUN (Figure 4E) of $Cre^{+}/ISG20^{fl/fl}$ mice after ischemia/reperfusion (I/R) were further elevated compared with those of $Cre^{-}/ISG20^{fl/fl}$ I/R mice. Hematoxylin and eosin (H&E) staining, immunohistochemical staining of the kidney tubule injury marker KIM-1, and terminal deoxynucleotidyl transferase dUTP nick-end labeling (TUNEL) staining demonstrated that tubule-specific ISG20 deficiency led to more severe morphological injury (Figures 4F and 4G) and increased renal TEC death (Figure 4H) in IRI mice. In addition, tubule-specific loss of ISG20 exacerbated renal inflammation in IRI mice, as shown by further enhancement of the levels of proinflammatory mediators and neutrophil and macrophage accumulation (Figure S3). Consistently, tubule-specific ISG20 deficiency aggravated renal dysfunction (Figures 4I and 4J) and histological lesions (Figure 4K) in mice after cisplatin injection.

Silencing or deficiency of ISG20 in renal TECs aggravated RNA oxidation under I/R conditions

In vitro, we found that both the mRNA and protein levels of ISG20 were induced by H/R treatment in HK-2 cells (Figures 5A and 5B). Immunofluorescence staining showed that ISG20 was located in the nucleolus and Cajal body in normal HK-2 cells, as evidenced by the colocalization of ISG20 with the nucleolar marker UBF1 and Cajal body marker Coilin, and translocated to the nucleoplasm in response to H/R treatment (Figure S4). Gene silencing of ISG20 was assessed by a short interfering RNA (siRNA) approach (Figure 5C), which enhanced the percentage of apoptotic HK-2 cells after hypotonic treatment with oxidized RNA (Figure 5D). In addition, lowering the expression of ISG20 resulted in elevated cell death (Figures 5E and S5A), caspase-3 activity (Figure 5F), and RNA oxidation (Figure 5G) in HK-2 cells with H/R treatment. When ISG20 expression was inhibited, more severe apoptosis and RNA oxidation were also observed in HK-2 cells treated with cisplatin (Figures S5B and S5C). *In vivo*, immunohistochemical staining and ELISA showed that tubule-specific ISG20 deficiency further exacerbated renal oxidized RNA levels in IRI mice (Figures 5H and 5I).

ISG20 contributed to the degradation of oxidized RNA through its exoribonuclease activity

We next investigated the effects of ISG20 overexpression on cell fate and RNA oxidation under I/R conditions. HK-2 cells were infected with adenovirus vectors harboring human ISG20 or $ISG20^{D94G}$ to mediate the overexpression of wild-type ISG20 and mutant ISG20 lacking 3′-5′-exoribonuclease activity (Figure 6A). Overexpression of ISG20 attenuated apoptosis or cell death of HK-2 cells after hypotonic treatment with oxidized RNA (Figure 6B) or H/R treatment (Figures 6C, 6D, and S6A). Moreover, the elevated levels of oxidized RNA in H/R-treated HK-2 cells were reduced by ISG20 overexpression (Figure 6E). However, $ISG20^{D94G}$ overexpression failed to reduce the levels of apoptosis and oxidative RNA in H/R-treated HK-2 cells (Figures 6B–6E and S6A). Similar results were also found in cisplatin-treated HK-2 cells (Figures S6B and S6C). The lack of inhibitory effects of catalytically inactive $ISG20^{D94G}$ on RNA oxidation supports the hypothesis that ISG20 exonuclease activity determines oxidized RNA degradation.

ISG20 restricted oxidized RNA-induced ER stress and UPR cascades

RNA oxidation potentially may lead to the accumulation of aberrant or misfolded proteins. Increased fluorescence intensity of the Aggresome detection reagent and more aggregated protein cargoes were observed in HK-2 cells with oxidized RNA hypotonic treatment (Figures S7A and S7B) assessed by flow cytometry and fluorescence microscopy. As a result, the ER stress/UPR cascades were activated in oxidized RNA hypotonic-treated HK-2 cells, as evidenced by enhanced phosphorylation of IRE1α and protein levels of CHOP (Figure S7C) and increased downstream mRNA splicing of XBP-1 and transcription of ATF4, CHOP, and Bip (Figure S7D). Importantly, enhanced formation of aggresomes containing unfolded or misfolded proteins and activated ER stress/UPR cascades observed in HK-2 cells with H/R treatment were inhibited by the

Figure 3. ISG20 was upregulated in kidneys from mice and patients with AKI

(A) Heatmap of exoribonuclease gene expression levels in the kidneys from Sham and IRI mice by RNA-seq analysis (n = 3). (B) Relative mRNA levels of PDE12 and ERI2 in the kidneys from Sham and IRI mice (n = 8). (C) Representative western blot gel documents and summarized data showing the protein levels of PDE12 and ERI2 in the kidneys from Sham and IRI mice (n = 8). (D) Relative mRNA levels of ISG20 in the kidneys from Sham and IRI mice (n = 8). (E) Representative western blot gel documents and summarized data showing the protein levels of ISG20 in the kidneys from Sham and IRI mice (n = 8). (F) Representative photomicrographs and quantification of ISG20 immunohistochemical staining in the kidneys from Sham and IRI mice (n = 8). Red arrows indicate representative ISG20 highly expressed cells ($ISG20^{high}$). (G) Relative mRNA levels of ISG20 in the kidneys from cisplatin-treated mice (n = 8). (H) Representative western blot gel documents and summarized data showing the protein levels of ISG20 in the kidneys from cisplatin-treated mice (n = 8). (I) Representative photomicrographs and quantification of ISG20 immunohistochemical staining in the kidneys from cisplatin-treated mice (n = 8). Red arrows indicate representative $ISG20^{high}$ cells. (J) Representative photomicrographs and quantification of ISG20 immunohistochemical staining in the kidneys from normal subjects (n = 7) and patients with ATN (n = 15). Red arrows indicate representative $ISG20^{high}$ cells. Data are represented as the mean ± SEM. $^{*}p < 0.05$, $^{**}p < 0.01$, $^{***}p < 0.001$; ns, not significant. See also Figure S2.

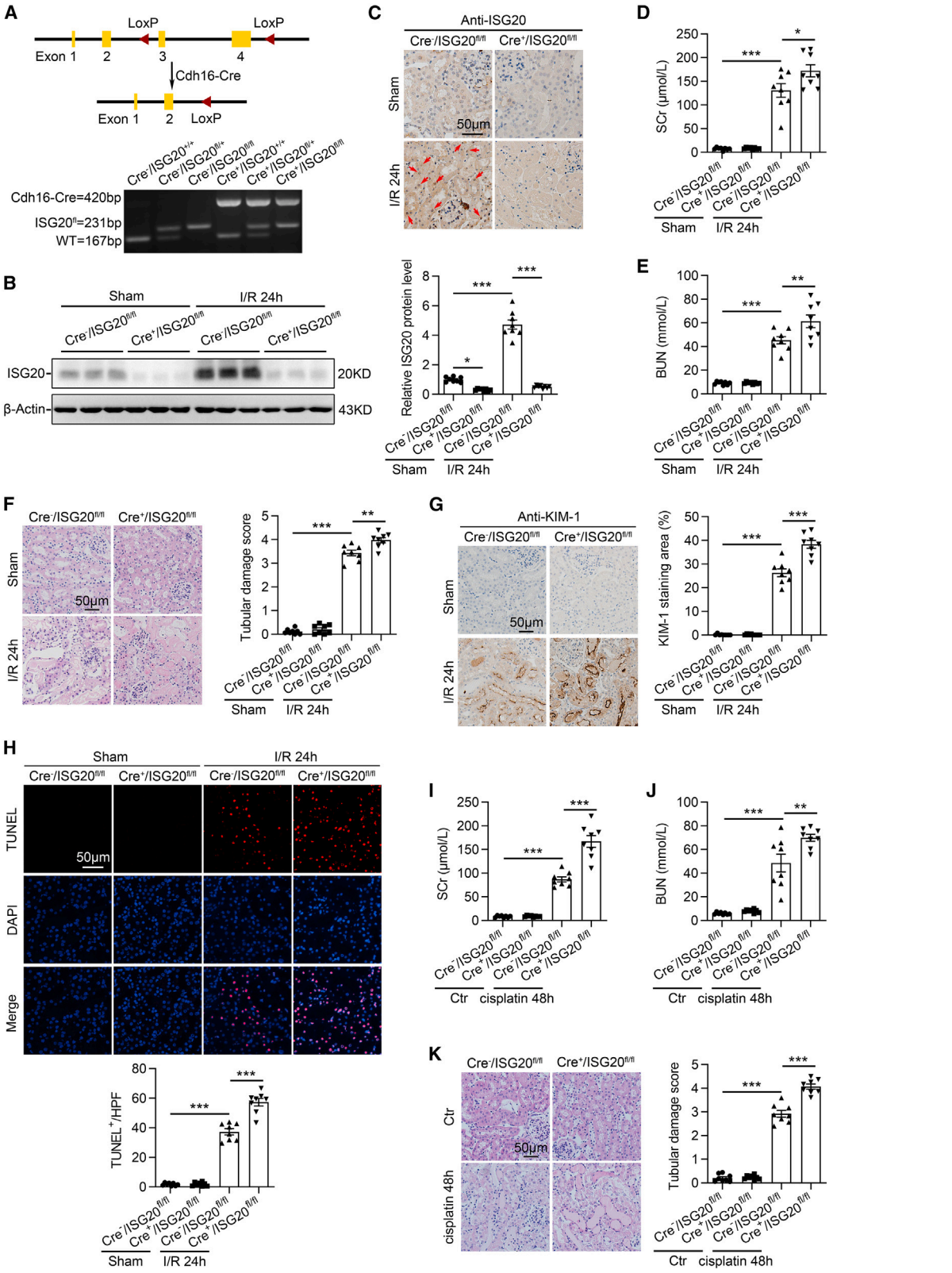

(legend on next page)

overexpression of wild-type human ISG20, but not ISG20^{D94G} (Figures 7A–7C). *In vivo*, western blot and real-time RT-PCR showed that the activated ER stress/UPR cascades in the kidneys of IRI mice were further exacerbated by tubule-specific ISG20 deficiency (Figures 7D and 7E).

Overexpression of ISG20 protected against renal IRI in mice

To examine the therapeutic potential of targeting ISG20 in IRI mice, recombinant adeno-associated virus 9 (AAV9) vectors harboring murine ISG20 (AAV-mISG20) were delivered into the kidney via intrarenal gene delivery. The efficiency of gene transfection was confirmed by the enhanced ISG20 expression in the kidneys from AAV-ISG20-infected mice compared with AAV-NC-infected mice (Figure S8). Overexpression of ISG20 significantly ameliorated the SCr and BUN levels (Figures 8A and 8B), renal injury (Figures 8C and S9A), TEC death (Figure 8D), and renal inflammation (Figures S9B–S9D) in IRI mice. Accordingly, ISG20 overexpression ameliorated renal oxidized RNA production (Figures 8E and 8F) and ER stress/UPR cascades in kidneys from IRI mice (Figures 8G–8I).

DISCUSSION

The aim of this study was to investigate the potential of a therapeutic strategy that targets RNA oxidation for the treatment of AKI. Compared with DNA, lipid, and protein oxidation, RNA oxidation has received little attention. In particular, the dynamics of RNA oxidation in the injured kidney and its contribution to AKI remain to be elucidated. In this study, we characterized for the first time that the levels of oxidized RNA were enhanced in the kidneys of ATN patients and AKI model mice and further determined that renal RNA oxidation is an early event in response to AKI insults. Importantly, we found that renal oxidized RNA levels are positively correlated with SCr and BUN levels, suggesting that renal RNA oxidation may contribute to the onset and progression of AKI and may serve as a candidate predictor of renal injury.

In this study, one of the most important findings is that we identified ISG20 as a central molecule responsible for the degradation of oxidized RNA in AKI. ISG20 is considered to be involved in the biogenesis and/or maturation of ribosomal RNA (rRNA) and small nuclear RNA because of the major subcellular location of ISG20 in the nucleolus and Cajal body.[16] Recent studies have highlighted the antiviral activity of ISG20 against a broad spectrum of RNA viruses by either directly degrading viral genomic RNA or exonuclease independently blocking viral mRNA translation.[17] According to our data, ISG20 is the only exoribonuclease exhibiting altered expression at both the mRNA and protein levels among all 5′-3′ and 3′-5′ exoribonucleases in the kidney from I/R mice. We also found that the nucleolus- and Cajal body-located ISG20 in HK-2 cells was expanded to the nucleoplasm under hypoxic conditions. The predominantly nuclear deposition of both oxidized RNA and ISG20 indicated a possible role of ISG20 in restricting RNA oxidation in AKI, which was verified by our *in vitro* and *in vivo* studies through ISG20-targeted intervention approaches. The ExoII motif of ISG20 mediates its enzymatic activity, which can be completely abolished by replacing aspartic acid 94 (D94) in the ExoII motif with glycine (D94G).[15] Notably, we confirmed that ISG20-mediated degradation of oxidized RNA relies on its 3′-5′ exoribonuclease activity in AKI, as evidenced by the failure of catalytically inactive mutant ISG20^{D94G} overexpression to reduce oxidized RNA levels under I/R conditions. Several lines of evidence have suggested the potential role of apurinic/apyrimidinic endodeoxyribonuclease 1 (APEX1) and polyribonucleotide nucleotidyltransferase 1 (PNPT1) in controlling oxidized RNA in human cells.[18,19] However, PNPT1 is predominantly localized in the mitochondrial intermembrane space,[20] which implies that it is insufficient for the complete degradation of the oxidized RNA mainly located in nucleus under I/R conditions. APEX1 is a multifunctional enzyme with 5′ apurinic endonuclease activity, 3′-5′ exonuclease, 3′-phosphodiesterase, 3′ RNA phosphatase, and 3′ exoribonuclease activities, which allows it to act on both DNA and RNA, but its 3′-5′ exoribonuclease activity against unstructured RNA is relatively weak.[21,22] Therefore, due to the functional importance of ISG20 in controlling oxidized RNA and its nuclear location and ssRNA preference, ISG20 may be a key restrictor of RNA oxidation in AKI.

The overproduced oxidized RNA and accompanying cell death observed in various diseases and pathological conditions suggest that RNA oxidation is a contributing factor in the process of cell death; however, compelling evidence is lacking.[4,5,23] In addition, the cellular responses to oxidized RNA have not been fully investigated.[24] Our study provides strong evidence that oxidized RNA triggers cell damage and renal injury in AKI. Direct evidence is the increased cell death and apoptosis of HK-2 cells after treatment with oxidized RNA generated from the Fenton reaction, the most pathophysiologically relevant reaction in mediating RNA oxidation.[25,26] Based on the ability of ISG20 to degrade oxidized RNA, ISG20 silencing aggravated HK-2 cell apoptosis when subjected to oxidized RNA or H/R

Figure 4. Tubule-specific ISG20 deletion in mice exacerbated renal injury after I/R

(A) Experimental scheme for generating tubule-specific ISG20 knockout mice (Cdh16-Cre^{+}/ISG20$^{fl/fl}$) by using the Cre-*loxP* recombination system. Genotyping was confirmed by tail preparation and PCR. (B) Representative western blot gel documents and summarized data showing the protein levels of ISG20 in the cortex of kidneys from different groups of IRI model mice (n = 8). (C) Representative photomicrographs of ISG20 immunohistochemical staining in the kidneys from different groups of IRI model mice (n = 8). (D) SCr levels of different groups of IRI model mice (n = 8). (E) BUN levels of different groups of IRI model mice (n = 8). (F) Representative photomicrographs of H&E staining and quantitative assessment of tubular damage in kidneys from different groups of IRI model mice (n = 8). (G) Representative photomicrographs and quantification of KIM-1 immunohistochemical staining in the kidneys from different groups of IRI model mice (n = 8). (H) Representative photomicrographs and quantification of terminal deoxynucleotidyl transferase-mediated uridine triphosphate nick-end labeling (TUNEL) assays of the kidneys from different groups of IRI model mice to assess renal cell death (n = 8). Nuclei were revealed by using DAPI staining. (I) SCr levels of different groups of cisplatin-induced AKI mouse model (n = 8). (J) BUN of different groups of cisplatin-induced AKI model mice (n = 8). (K) Representative photomicrographs of H&E staining and quantitative assessment of tubular damage in kidneys from different groups of cisplatin-induced AKI model mice (n = 8). Data are represented as the mean ± SEM. *$p < 0.05$, **$p < 0.01$, ***$p < 0.001$. See also Figure S3.

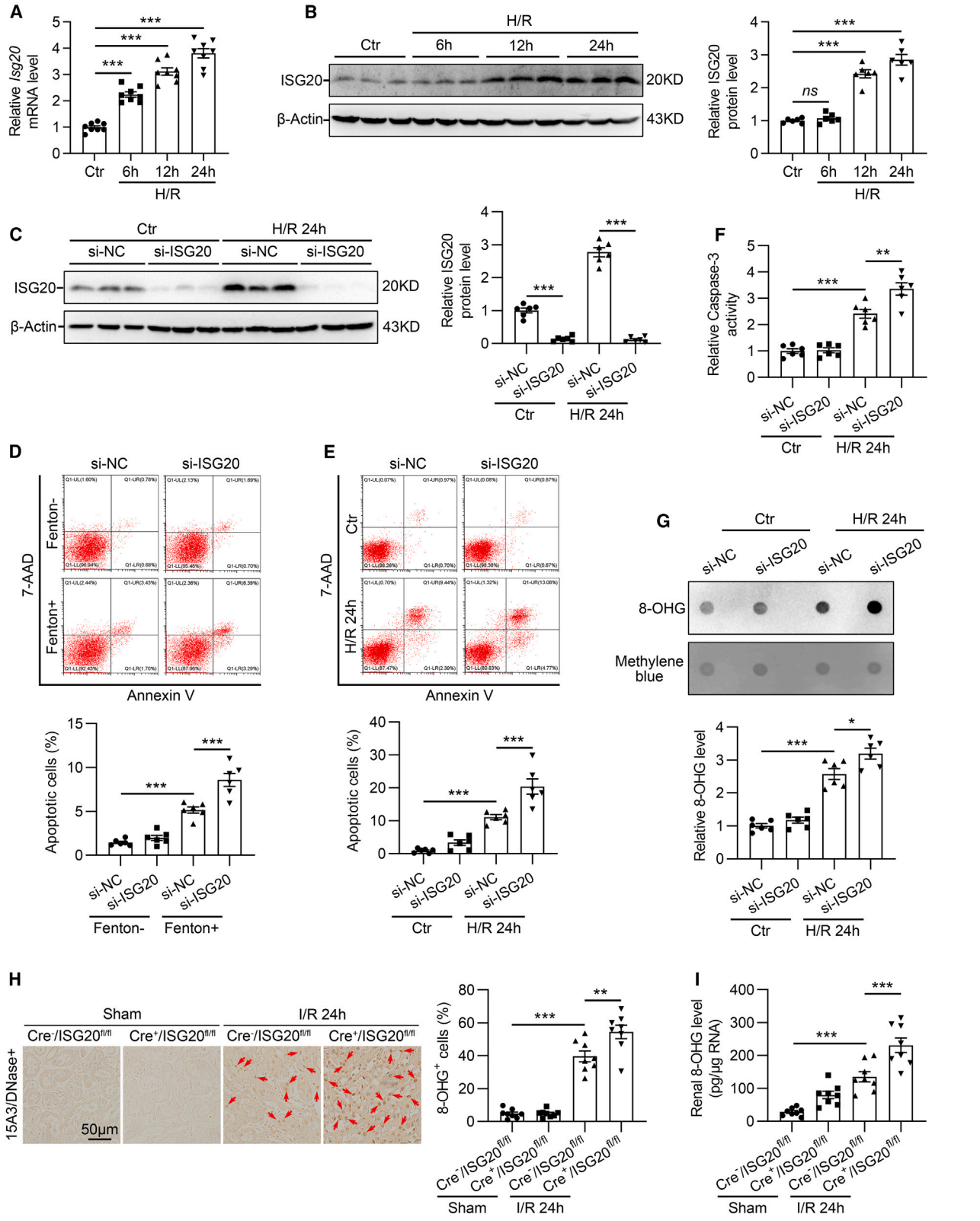

(legend on next page)

treatment, and tubule-specific ISG20 deficiency exacerbated renal susceptibility to IRI in mice; ISG20 overexpression instead exerted a protective role in these *in vitro* and *in vivo* models. The above ISG20-targeted intervention studies highlight a decisive role of oxidized RNA in the initiation and progression of AKI. Moreover, the beneficial effects of ISG20 overexpression on RNA oxidation and renal injury suggest a promising therapeutic strategy for the treatment of AKI by targeting ISG20-controlled RNA oxidation.

Another important issue is how oxidized RNA exerts its cytotoxicity, which remains unclear. Oxidative lesions in rRNA, tRNA, and mRNA primarily lead to strand breaks and oxidative base modifications, altering their structure and function, which may interfere with the protein translation process and frequently result in the production of unfolded or misfolded proteins and protein aggresome accumulation within the cells.[4–6] The accumulation of unfolded or misfolded proteins in the ER lumen is a condition referred to as ER stress, which activates the IRE1, PERK, and ATF6 signaling pathways, three principal branches of the UPR to restore ER homeostasis.[27] However, unfolded or misfolded protein overload and prolonged UPR induce ER stress-associated apoptosis.[28–30] Accumulating evidence has described the importance of ER stress in the pathogenesis of AKI and probably also in AKI-to-CKD progression.[31] Our data showed that oxidized RNA or H/R treatment resulted in enhanced protein aggresome formation and activated ER stress/UPR/apoptotic pathways, which can be inhibited by the overexpression of ISG20 depending on its 3′–5′ exoribonuclease activity. Moreover, I/R-induced renal ER stress and UPR were also prevented by ISG20 overexpression. These experimental data addressed the molecular mechanisms by which oxidized RNA causes TEC apoptosis and renal injury under I/R conditions.

In this study, the transcriptional regulation mechanism of ISG20 in AKI is still lacking. Interferon (IFN) regulatory factor 1 (IRF1) is a master regulator of ISG transcription,[32] which can mediate IFN-induced ISG20 transcription by binding to an interferon-stimulated response element in the ISG20 gene promoter region.[33] Interestingly, early upregulated IRF1 expression in proximal tubule cells of I/R mice and ROS-treated tubular cells has been reported, and ROS-induced IRF1 in renal tubules is required for maximal ischemic AKI.[34] Thus, the upregulated expression of ISG20 in TECs under I/R conditions may be attributed to the ROS-stimulated IRF1 signaling pathway and seems to be an endogenous compensatory mechanism in response to oxidative stress in AKI; however, it is insufficient to resist quickly and sharply enhanced RNA oxidation. According to our data, overexpression of ISG20 before AKI induction protected against renal injury and endogenously compensative ISG20 was insufficient to resist the established AKI, suggesting that the timing of ISG20 overexpression is more important for renal protection than the ISG20 expression level. Therefore, encouraging the expression or activity of ISG20 at the early stage may be an opportunity for AKI treatment, and even a preventive measure for cardiac surgery-associated AKI and sepsis-associated AKI.

Moreover, many details of ISG20-mediated oxidized RNA degradation have not been addressed in this study. Does ISG20 need the assistance of oxidized RNA-specific binding proteins, such as Y box-binding protein 1,[35] HNRNPD, SF3B4, HNRNPC, and DAZAP1,[36] to discriminate the oxidized RNA from normal RNA? Does ISG20 have a preference for oxidized mRNA, tRNA, or rRNA? Whether certain RNA helicase is needed to unwind the double-stranded region and strong secondary structures within RNA before ISG20 exerts its exoribonuclease activity preferring ssRNA? All these questions will be interesting areas of investigation for future studies.

Collectively, these findings demonstrate for the first time that RNA oxidation participates in the pathogenesis of AKI and that the 3′-5′ exoribonuclease ISG20 is responsible for the degradation of oxidized RNA, which, at least in part, restricts the production of unfolded or misfolded proteins and the subsequent UPR and ER stress-related apoptosis. Our findings extend the knowledge of RNA oxidation in pathophysiology and advance the mechanisms of cells handling oxidized RNA. Modulation of the oxidized RNA handling mechanism by targeting ISG20 may provide a novel approach for the treatment of AKI.

MATERIALS AND METHODS

Human renal biopsy samples

Renal biopsies were performed as part of routine clinical diagnostic investigation, and the samples were obtained from the Department of Pathology, Shandong University School of Basic Medical Sciences. We collected human renal biopsy samples from patients with biopsy-proven ATN, as described in Table S1. None of these patients had started dialysis therapy at the time of kidney biopsy. Normal control samples were obtained from healthy kidney poles of individuals who underwent tumor nephrectomies or renal cystectomy without other

Figure 5. Silencing or deficiency of ISG20 in renal tubular epithelial cells aggravated RNA oxidation in response to AKI insults

(A) Relative mRNA levels of ISG20 in HK-2 cells with H/R treatment (n = 6). (B) Representative western blot gel documents and summarized data showing the protein levels of ISG20 in HK-2 cells with H/R treatment (n = 6). (C) Representative western blot gel documents and summarized data showing the protein levels of ISG20 in si-NC- or si-ISG20-transfected HK-2 cells with or without H/R treatment (n = 6). (D) Representative flow cytometry analysis and quantitative data depicting the apoptosis of si-NC- or si-ISG20-transfected HK-2 cells with oxidized RNA hypotonic treatment (n = 6). (E) Representative flow cytometry analysis and quantitative data depicting the apoptosis of si-NC- or si-ISG20-transfected HK-2 cells with H/R treatment (n = 6). (F) Summarized data showing caspase-3 activity in si-NC- or si-ISG20-transfected HK-2 cells with H/R treatment (n = 6). (G) Representative RNA dot blot documents and summarized data showing the relative 8-OHG levels of RNA extracts from si-NC- or si-ISG20-transfected HK-2 cells with H/R treatment (n = 6). (H) Representative photomicrographs of 15A3 antibody immunohistochemical staining of kidney sections with DNase treatment and quantification of 8-OHG$^+$ cells in kidneys from different groups of IRI model mice (n = 8). Red arrows indicate representative 8-OHG$^+$ cells. (I) Renal 8-OHG levels of different groups of IRI model mice (n = 8). Data are represented as the mean ± SEM. *$p < 0.05$, **$p < 0.01$, ***$p < 0.001$; ns, not significant. See also Figures S4 and S5.

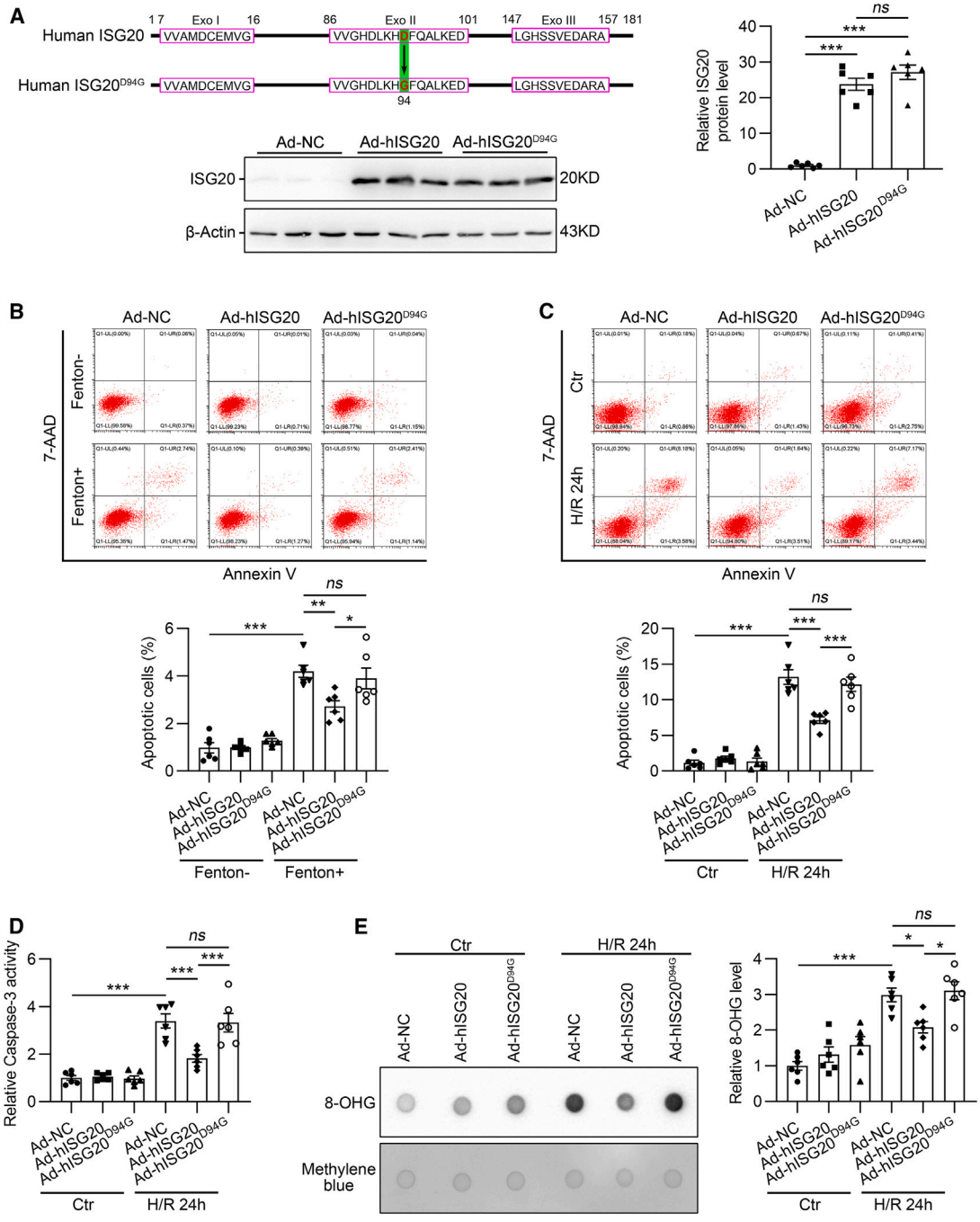

Figure 6. A single point mutation in the active site (ISG20^{D94G}) abolished ISG20-mediated oxidized RNA restriction

(A) Schematic representation of the three exonuclease active motifs (Exo I, II, and III) of human ISG20 (shown in pink boxes). The Asp94 residue (highlighted in red) of wild-type ISG20 was replaced with Gly to generate the catalytically inactive mutant ISG20^{D94G} (upper left). Representative western blot gel documents (lower) and summarized data (right) showing the protein levels of wild-type human ISG20 and mutant human ISG20^{D94G} in HK-2 cells after adenovirus vector (Ad-NC, Ad-hISG20, or Ad-hISG20^{D94G}) infection (n = 6). (B) Representative flow cytometry analysis and quantitative data depicting the apoptosis of adenovirus vector-infected HK-2 cells with oxidized RNA hypotonic treatment (n = 6). (C) Representative flow cytometry analysis and quantitative data depicting the apoptosis of adenovirus vector-infected HK-2 cells with H/R treatment (n = 6). (D) Summarized data showing caspase-3 activity in adenovirus vector-infected HK-2 cells with H/R treatment (n = 6). (E) Representative RNA dot blot documents and summarized data showing the relative 8-OHG levels of RNA extracts from adenovirus vector-infected HK-2 cells with H/R treatment (n = 6). Data are represented as the mean ± SEM. *p < 0.05, **p < 0.01, ***p < 0.001; ns, not significant. See also Figure S6.

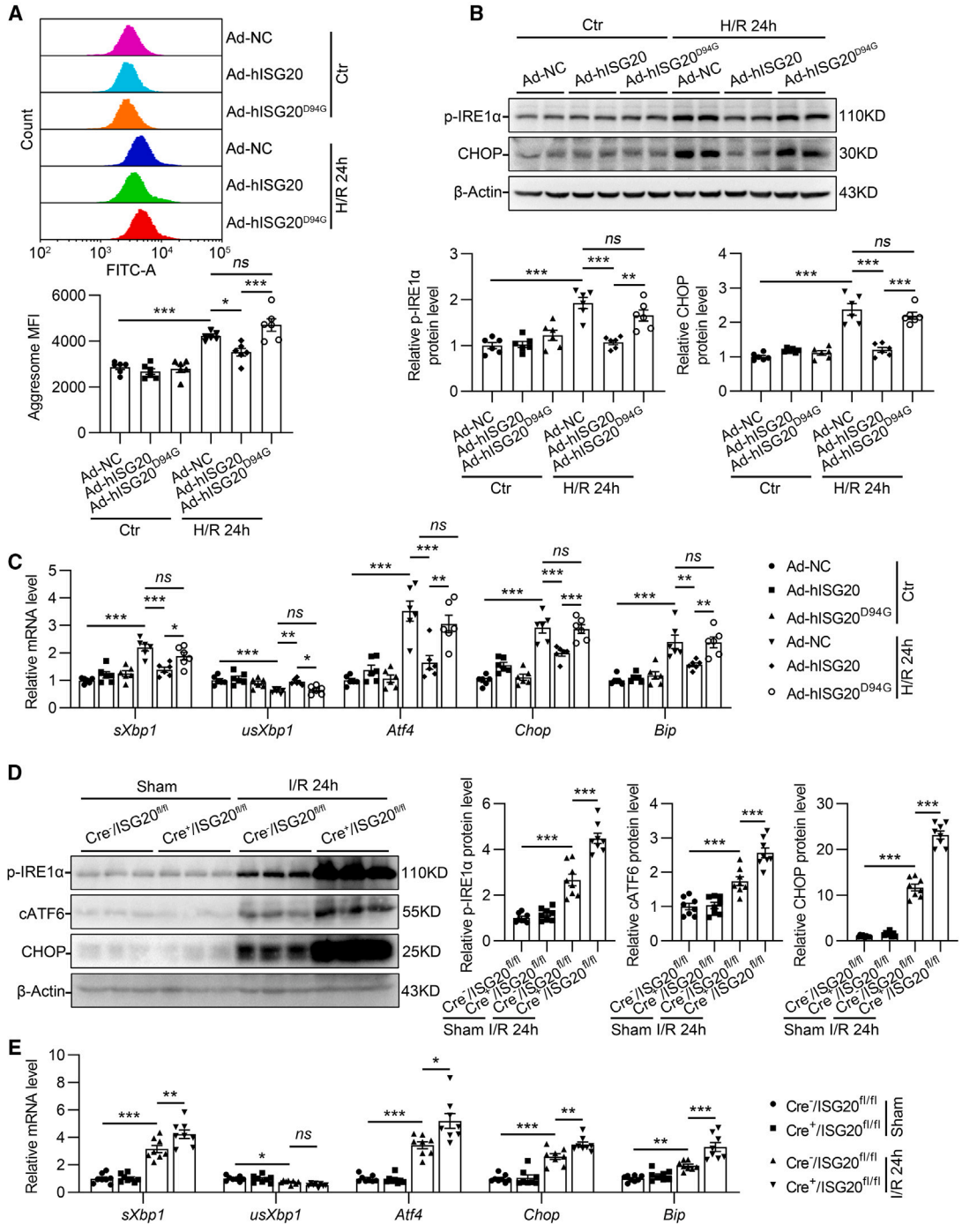

Figure 7. ISG20 restricted oxidized RNA-induced ER stress and UPR cascades

(A) Representative flow cytometry analysis and quantitative MFI depicting protein aggresomes in Ad-NC-, Ad-hISG20-, or Ad-hISG20^{D94G}-infected HK-2 cells with H/R treatment (n = 6). (B) Representative western blot gel documents and summarized data showing the protein levels of p-IRE1α and CHOP in Ad-NC-, Ad-hISG20-, or Ad-hISG20^{D94G}-infected HK-2 cells with H/R treatment (n = 6). (C) Relative mRNA levels of ER stress/UPR cascade downstream genes in Ad-NC-, Ad-hISG20-, or Ad-hISG20^{D94G}-infected HK-2 cells with H/R treatment (n = 6). (D) Representative western blot gel documents and summarized data showing the protein levels of p-IRE1α, cleaved ATF6 (cATF6), and CHOP in the kidneys from different groups of IRI model mice (n = 8). (E) Relative mRNA levels of ER stress/UPR cascade downstream genes in the kidneys from different groups of IRI model mice (n = 8). Data are represented as the mean ± SEM. *p < 0.05, **p < 0.01, ***p < 0.001; ns, not significant. See also Figure S7.

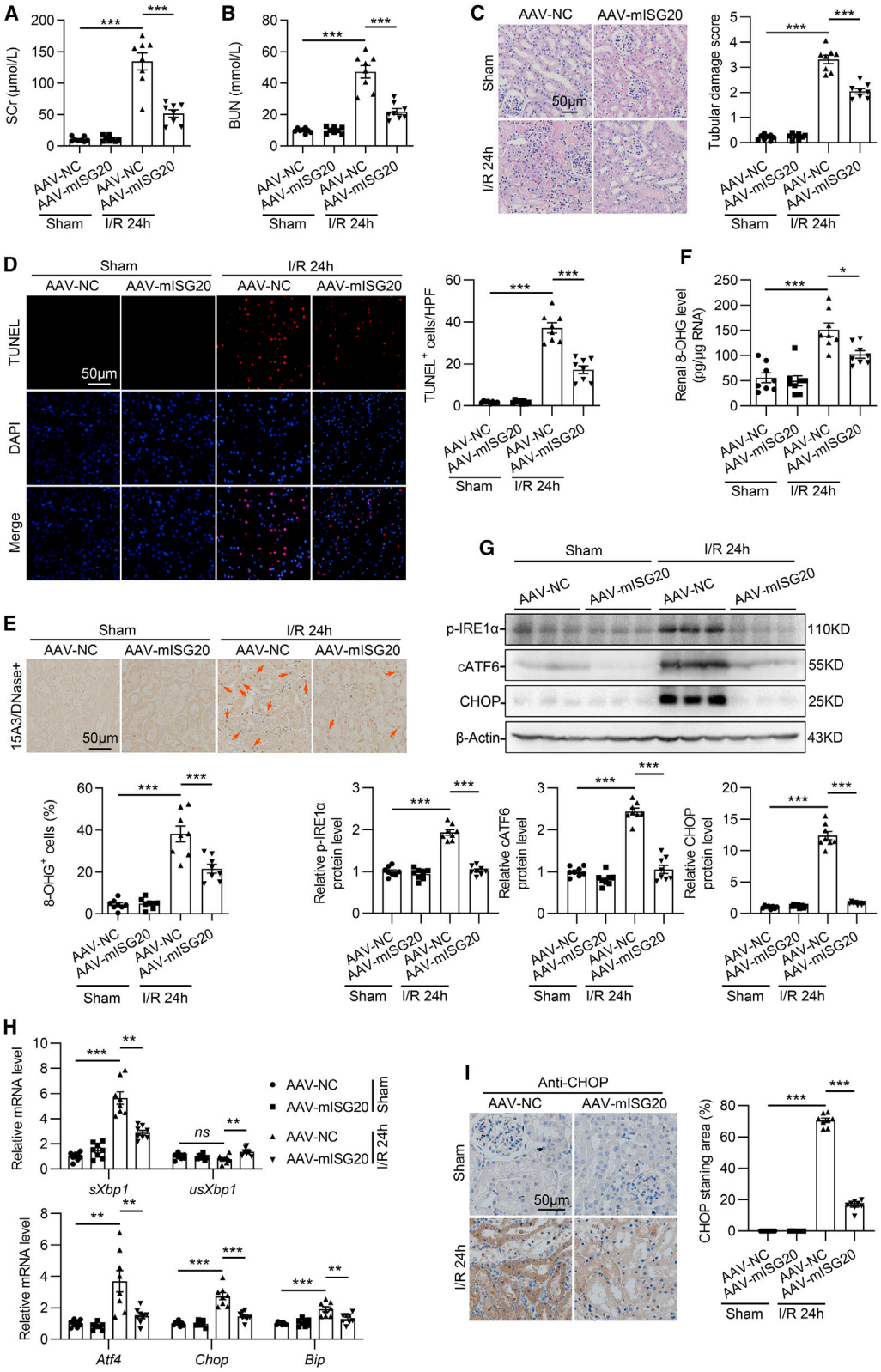

(legend on next page)

kidney diseases. The investigations were conducted in accordance with the principles of the Declaration of Helsinki and were approved by the Research Ethics Committee of Shandong University after informed consent was obtained from the patients.

Animal studies

All experimental protocols for animal studies were approved by the Institutional Animal Care and Use Committee of the School of Basic Medical Sciences, Shandong University (document no. ECSBMSSDU2019-2-024) and conducted in accordance with the National Institutes of Health Guide for the Care and Use of Laboratory Animals. Different groups were allocated in a randomized manner and investigators were blinded to the allocation of different groups when performing surgeries and outcome evaluations. All mice (five mice per cage) were housed under standard laboratory conditions (12 h on/off; lights on at 7:00 a.m.) and temperature (24°C) with *ad libitum* access to water and standard laboratory chow diet (Beijing Keao Xieli Feed, Beijing, China). Water and cages were autoclaved. Cages with standard corncob bedding were changed three times a week. For all of the *in vivo* experiments, littermate control mice were used. The mouse genotype did not cause visible changes in initial weight, health, or immune status. In all of the experiments, considering that female mice are resistant to renal ischemia reperfusion injury, only male mice were used. The number of mice used for the experiments is indicated for each experiment in the figure legends. All of our experimental animals were kept under barrier conditions under constant veterinary supervision and did not display any signs of distress or pathological changes that warranted veterinary intervention.

Generation of tubule-specific ISG20 knockout mice

Floxed ISG20 mice (C57BL/6N-*Isg20*$^{em1(flox)Cya}$, stock no. S-CKO-12340, Suzhou, China) were hybridized with transgenic mice expressing Cre-recombinase under the cadherin 16 promoter (B6.Cg-Tg (Cdh16-Cre) 91Igr/J, stock no. 012237, Jackson Laboratory, Bar Harbor, ME) to generate tubule-specific ISG20 knockout mice (Cdh16-Cre^{+}/ISG20$^{fl/fl}$; Cre^{+}/ISG20$^{fl/fl}$). Age-matched mice without Cre (Cdh16-Cre^{-}/ISG20 $^{fl/fl}$; Cre^{-}/ISG20 $^{fl/fl}$) were used as controls. Mouse genotyping was performed using genomic DNA isolated from mouse tails by PCR. The specific primers for tail PCR genotyping in this study are listed in Table S2. Flox genotyping produced 231 and 167 bp fragments for the mutant and wild type, respectively. Wild-type yields only a 167 bp band, homozygous (ISG20 $^{fl/fl}$) yields only a 231 bp band, and heterozygous (ISG20$^{fl/+}$) yields both bands. Cre-positive (Cre^{+}) yields a 420 bp band, but Cre-negative (Cre^{-}) has no band.

Mouse models of AKI

A mouse model of renal IRI was established as described previously.[37] In brief, 8-week-old male mice (average weight of 20 ± 2 g) were anesthetized with intraperitoneal pentobarbital sodium (50 mg/kg body weight), and a midline abdominal incision was made. For IRI mice, bilateral renal pedicles were clipped for 30 min using microaneurysm clamps. At the end of the ischemic period, the vascular clamps were removed (reperfusion) and the kidneys were observed for 5 min to document reflow. The incision was then closed and the animal was allowed to recover. During the ischemic period, body temperature was maintained between 36°C and 37.5°C using a temperature-controlled heating system. Sham-operated mice underwent the same operation without renal pedicle clamping. At the indicated time after reperfusion, blood samples were obtained via cardiac puncture and anesthetized mice were perfused with phosphate-buffered saline (PBS) at 150–160 mm Hg via a butterfly 23G needle inserted into the left ventricle to completely remove blood. One kidney was then harvested and the other kidney was further perfused with 4% paraformaldehyde for histopathological analysis. To determine the renal oxidized RNA and ISG20 levels in the IRI model, 8-week-old male wild-type C57BL/6N mice (n = 32), purchased from Beijing Vital River Laboratory Animal Technology, were randomly allocated into four groups (n = 8/group) as follows: (1) Sham-operated group, (2) I/R 6 h group, (3) I/R 12 h group, and (4) I/R 24 h group. To determine the role of tubule-specific ISG20 deficiency in the IRI model, 8-week-old male Cre^{-}/ISG20$^{fl/fl}$ mice (n = 16) and Cre^{+}/ISG20$^{fl/fl}$ mice (n = 16) were randomly allocated into four groups (n = 8/group) as follows: (1) Sham-operated Cre^{-}/ISG20$^{fl/fl}$ group, (2) Sham-operated Cre^{+}/ISG20$^{fl/fl}$ group, (3) I/R 24 h Cre^{-}/ISG20$^{fl/fl}$ group, and (4) I/R 24 h Cre^{+}/ISG20$^{fl/fl}$ group.

AKI in mice was also induced by a single intraperitoneal injection of cisplatin at a dose of 30 mg/kg (Sigma, St. Louis, MO), while the control mice were injected with an equal volume of saline. At the indicated time after injection, mice were sacrificed, and blood and kidney samples were collected for various analyses. To determine the renal oxidized RNA and ISG20 levels in the cisplatin-induced AKI model, 8-week-old male wild-type C57BL/6N mice (n = 32) were randomly allocated into four groups (n = 8/group) as follows: (1) control group,

Figure 8. ISG20 overexpression in mice significantly ameliorated renal injury after I/R

(A) SCr levels of different groups of IRI model mice (n = 8). (B) BUN levels of different groups of IRI model mice (n = 8). (C) Representative photomicrographs of H&E staining and quantitative assessment of tubular damage in kidneys from different groups of IRI model mice (n = 8). (D) Representative photomicrographs and quantification of TUNEL assays of the kidneys from different groups of IRI model mice to assess renal cell death (n = 8). Nuclei were revealed by using DAPI staining. (E) Representative photomicrographs of 15A3 antibody immunohistochemical staining of kidney sections with DNase treatment and quantification of 8-OHG^{+} cells in kidneys from different groups of IRI model mice (n = 8). Red arrows indicate representative 8-OHG^{+} cells. (F) Renal 8-OHG levels of different groups of IRI model mice (n = 8). (G) Representative western blot gel documents and summarized data showing the protein levels of p-IRE1α, cleaved ATF6 (cATF6), and CHOP in the kidneys from different groups of IRI model mice (n = 8). (H) Relative mRNA levels of ER stress/UPR cascade downstream genes in the kidneys from different groups of IRI model mice (n = 8). (I) Representative photomicrographs and quantification of CHOP immunohistochemical staining in the kidneys from different groups of IRI model mice (n = 8). Data are represented as the mean ± SEM. *p < 0.05, **p < 0.01, ***p < 0.001. See also Figures S8 and S9.

(2) cisplatin 24 h group, (3) cisplatin 48 h group, and (4) cisplatin 72 h group. To determine the role of tubule-specific ISG20 deficiency in the cisplatin-induced AKI model, 8-week-old male $Cre^{-}/ISG20^{fl/fl}$ mice (n = 16) and $Cre^{+}/ISG20^{fl/fl}$ mice (n = 16) were randomly allocated into four groups (n = 8/group) as follows: (1) $Cre^{-}/ISG20^{fl/fl}$ control group, (2) $Cre^{+}/ISG20^{fl/fl}$ control group, (3) $Cre^{-}/ISG20^{fl/fl}$ cisplatin 48 h group, and (4) $Cre^{+}/ISG20^{fl/fl}$ cisplatin 48 h group.

Assessment of renal function

High-performance liquid chromatography (HPLC) was performed to measure SCr using an Agilent 1100 HPLC system (Agilent Technologies, Santa Clara, CA). The procedure was performed as described previously.[38,39]

siRNA-mediated gene silencing

Cells were cultured in medium without antibiotics. siRNA for target genes or negative control siRNA were delivered into cells by the Lipofectamine 2000 reagent (Invitrogen, Carlsbad, CA) following the manufacturer's protocol. siRNA targeting sequence: 5′-GCUACACAAU CUACGACACTT-3′; 3′-GUGUCGUAGAUUGUGUAGCTT-5′.

Intrarenal AAV delivery

Recombinant AAV9 constructs of murine ISG20 (AAV-mISG20) and their negative controls (AAV-NC) were designed and purchased from ViGene Biosciences (Shandong, China). Eight-week-old male wild-type C57BL/6N mice (n = 32) were randomly allocated into four groups (n = 8/group) as follows: (1) AAV-NC Sham group, (2) AAV-mISG20 Sham group, (3) AAV-NC I/R 24 h group, and (4) AAV-mISG20 I/R 24 h group. The titers of recombinant AAV-NC and AAV-mISG20 were approximately 5.25×10^{13} viral genomes/mL and 6×10^{11} viral genomes of AAV-NC and AAV-mISG20 were delivered to the kidney by intraparenchymal injection. The procedure for intraparenchymal delivery was performed as described previously.[40–42] Preliminary studies indicated that AAV-mediated GFP expression in the kidney parenchyma was significantly upregulated after 1 month, and no toxicity was observed in AAV-treated mice.

Histology examination

Formalin-fixed kidney sections were stained with H&E. The percentage of tubules in the corticomedullary junction that displayed cellular necrosis and loss of brush border were counted and scored in a blinded manner as follows: 0, none; 1, 0%–10%; 2, 11%–25%; 3, 26%–45%; 4, 46%–75%; and 5, >75%. At least 10 high-power fields per section for each sample were examined. Immunohistochemistry analysis and immunofluorescence staining were performed as described in our previous study.[43,44] For the immunohistochemistry analysis of 8-OHG, kidney sections were pretreated with or without DNase I (1 U/μL) for 1 h before the staining procedure. For immunofluorescence staining with biotinylated LTL (Vector Labs, B-1325-2), Alexa Fluor 488-conjugated streptavidin (Yeasen Biotechnology, 35103ES60) was used according to the manufacturer's instructions. Negative controls using isotype-matched normal IgG were used to check for antibody specificity. The antibodies used in this study are summarized in Table S3.

TUNEL assay

Cell death in the kidney section was detected by TUNEL assay following the manufacturer's protocol (Roche Diagnostics, Mannheim, Germany).

Cell culture and treatment

Immortalized human renal proximal tubule (HK-2) cells (American Type Culture Collection, Manassas, VA) were cultured as described previously.[45] *In vitro* H/R was induced by incubating HK-2 cells in a hypoxic environment for 2 h (0.1% O_2) followed by reoxygenation at different time points. *In vitro* cisplatin treatment was induced by incubating HK-2 cells with cisplatin (50 μM) for 48 h.

RNA extraction and real-time quantitative PCR

Total RNA was isolated from kidney tissues (10–15 mg of frozen kidney tissue per mouse) and HK-2 cells using TRIzol reagent (Invitrogen). The mRNA expression levels were determined by real-time quantitative RT-PCR using a Bio-Rad iCycler system (Bio-Rad, Hercules, CA). The specific primers for target genes in this study are listed in Table S2. Levels of the housekeeping gene β-actin were used as an internal control for the normalization of RNA quantity and quality differences among the samples.

Oxidation of RNA by the Fenton reaction

Two hundred micrograms of RNA sample was incubated in an iron solution (200 μM $FeCl_2$ and 200 μM ferric citrate in 12.5 mM MES buffer [pH 6.6]) at 4°C for 5 min and then hydrogen peroxide (10 mM final concentration) was added. After incubation for 30 min at 37°C, the reaction was terminated with deferoxamine (10 mM final concentration) and chilled on ice for 5 min. The oxidized RNA was precipitated with 3 M sodium acetate (pH 5.2) and 100% ethanol. The pellet was washed with 75% ethanol and dried for 5 min. It was resuspended in 20 μL of 0.1% diethylpyrocarbonate-treated water.

The HK-2 cells were plated in six-well plates and incubated under 5% CO_2 at 37°C for 24 h and then subjected to hypotonic treatment with 10 μg normal or oxidized RNA in a buffer solution (30 mM KCl and 10 mM Hepes-NaOH [pH 7.4]) and were incubated under 5% CO_2 at 37°C for 5 min as described previously.[46] The medium was then changed to F12 supplemented with 10% FBS for an additional 24 h incubation.

OxiSelect oxidative RNA damage ELISA kit assay

The reagents were prepared and mixed thoroughly before use. One microgram of renal RNA extracts was digested into nucleosides by incubating the sample with 5–20 units of nuclease P1 for 2 h at 37°C in 20 mM sodium acetate (pH 5.2), followed by treatment with 5–10 units of alkaline phosphatase for 1 h at 37°C in 100 mM Tris (pH 7.5). The reaction mixture was centrifuged for 5 min at 6,000 × *g*, and the supernatant was used for the 8-OHG assay. Then, the RNA samples or 8-OHG standards were added to the wells

of the 8-OHG conjugate-coated plate. The plate was incubated at room temperature for 10 min on an orbital shaker. Then, 50 μL of the diluted anti-8-OHG antibody was added to each well and incubated at room temperature for 1 h on an orbital shaker. Microwell strips were washed three times with 250 μL 1× wash buffer per well with thorough aspiration between each wash. After the last wash, empty wells and tap microwell strips were placed on an absorbent pad or paper towel to remove excess 1× wash buffer. Then, 100 μL of the diluted secondary antibody-enzyme conjugate was added to all wells and incubated at room temperature for 1 h on an orbital shaker. The microwell strips were washed three times according to the above steps. Then, 100 μL of substrate solution was added to each well, including the blank wells, and incubated at room temperature on an orbital shaker. The actual incubation time may vary from 2 to 30 min. The enzyme reaction was stopped by adding 100 μL of stop solution into each well, including the blank wells. The data were analyzed immediately. The absorbance of each microwell was read on a spectrophotometer using 450 nm as the primary wavelength.

Western blot analyses

Tissues as well as cell pellets from culture were resuspended in RIPA buffer containing 1× protease inhibitor cocktail, 1× phenylmethylsulfonyl fluoride, and 1× phosphatase inhibitor 1 and 2. Tissue lysates and cell lysates were incubated on ice for at least 10 min to ensure proper cell lysis before centrifugation of lysates at 4°C for 15 min at 12,000 × *g*. Following centrifugation, soluble supernatant was carefully transferred to a fresh Eppendorf tube, and protein concentration determination was carried out using a BCA protein assay. Proteins were separated by 8% or 10% SDS-PAGE and transferred onto PVDF membranes. Then, selected proteins were probed with antibodies as indicated. The antibodies used in this study are summarized in Table S3. To document the loading controls, the membrane was reprobed with a primary antibody against the housekeeping protein β-actin.

RNA dot blot

Total RNA was extracted from HK-2 cells according to the manufacturer's instructions. The RNA dot blot assay was executed following a published protocol with appropriate modifications. In brief, diluted RNA was heated at 95°C for 3 min to disrupt secondary structure and then cooled down. The cold RNA samples were loaded on Amersham Hybond-N^+ membrane (GE Healthcare), dried, and fixed by UV crosslinking. The membrane was blocked with 5% nonfat dry milk (in 1× PBST) for 1–2 h and incubated with anti-DNA/RNA Damage antibody [15A3] antibody (1:1,000, Santa Cruz, Dallas, TX) overnight at 4°C. After washing, the membrane was incubated with HRP-conjugated goat anti-mouse IgG (1:5,000 dilution) for 1 h at room temperature. Blots were exposed with Pierce ECL Western Blotting Substrate (Thermo Fisher Scientific).

Apoptotic cell detection

Cell apoptosis was determined by allophycocyanin (APC)-conjugated Annexin V and 7-AAD staining as described.[41] The cells were harvested and resuspended in 200 μL of Annexin V binding buffer containing 5 μL of 7-AAD and 5 μL of Annexin V-APC for 15 min at room temperature in the dark. Cells were then washed and resuspended in phosphate-buffered saline. Acquisition was performed on a Cytoflex S flow cytometer, and data were analyzed using CytExpert Program (both from Beckman Coulter).

Aggresome detection

According to the manufacturer's instructions, reconstituted lyophilized MG-132 (120 nmol) in 12 μL DMSO was prepared as a 10 mM stock solution. For use as a positive control, MG-132 was diluted to 5 μM in the culture medium and cells grown for 6 h and centrifuged at 400 × *g* for 5 min to pellet the cells. The cells were carefully resuspended and washed with 1 mL of 1× PBS. Using a micropipette, the cell suspension was added dropwise into 1 mL of 4% formaldehyde solution contained in a 15 mL conical tube. The fixative was slowly vortexed during the addition of the cell suspension. The mixture was allowed to stand for 30 min at room temperature. The fixed cells were collected by centrifugation at 800 × *g* for 10 min. The cell pellet was resuspended in the remaining small volume of supernatant using a micropipette, 1 mL of 1× PBS was added to the cells, and they were centrifuged at 800 × *g* for 10 min. The cell pellets were resuspended in 500 μL of freshly diluted Aggresome Red Detection Reagent. Samples were protected from light and incubated for 30 min at room temperature. The samples were analyzed in the fluorescein isothiocyanate channel of a flow cytometer (Beckman Coulter).

Statistics

Data are expressed as the mean ± SEM. Statistical analyses were performed with GraphPad Prism (v.8.0, GraphPad Software, San Diego, CA). The normality assumption of the data distribution was assessed using the Kolmogorov-Smirnov test. Comparisons between two groups were performed using two-tailed Student's t test for normally distributed data and Mann-Whitney rank-sum test for nonnormally distributed data. Differences between multiple groups with one variable were determined using one-way ANOVA followed by post hoc Tukey's test. To compare multiple groups with more than one variable, two-way ANOVA followed by post hoc Tukey's test was used. For correlation analysis, the Pearson correlation coefficient was applied as appropriate.

DATA AND CODE AVAILABILITY

RNA sequencing datasets have been deposited to the Gene Expression Omnibus under accession code GSE226275. Other data that support the findings of this study are available from the corresponding authors upon reasonable request.

SUPPLEMENTAL INFORMATION

Supplemental information can be found online at https://doi.org/10.1016/j.ymthe.2023.07.008.

ACKNOWLEDGMENTS

This study was supported by the National Key R&D Program of China (2020YFC2005000) and the National Natural Science Foundation of China (82090024, 91949202, 81970580, 82270718, and 82100749).

AUTHOR CONTRIBUTIONS

M.J., L.L., and R.C. conducted *in vivo* and *in vitro* experiments, performed data analysis, and helped write the manuscript. J.D., Z.Q., and D.Z. contributed to the experimental design and performed *in vitro* experiments. X.W. and J.W. performed *in vivo* animal studies. M.L., Y.X., Y.S., Y.Z., Z.W., T.Z., H.H., and J.S. helped design the experiments. M.J. and Z.W. analyzed human renal biopsy samples. F.Y. and W.T. designed the experiment, interpreted the data, wrote the manuscript, and approved the final version of the manuscript for publication.

DECLARATION OF INTERESTS

The authors declare no competing interests.

REFERENCES

1. Tang, C., Cai, J., Yin, X.M., Weinberg, J.M., Venkatachalam, M.A., and Dong, Z. (2021). Mitochondrial quality control in kidney injury and repair. Nat. Rev. Nephrol. *17*, 299–318.
2. Dennis, J.M., and Witting, P.K. (2017). Protective Role for Antioxidants in Acute Kidney Disease. Nutrients *9*, 718.
3. Tomsa, A.M., Alexa, A.L., Junie, M.L., Rachisan, A.L., and Ciumarnean, L. (2019). Oxidative stress as a potential target in acute kidney injury. PeerJ *7*, e8046.
4. Kong, Q., and Lin, C.L.G. (2010). Oxidative damage to RNA: mechanisms, consequences, and diseases. Cell. Mol. Life Sci. *67*, 1817–1829.
5. Poulsen, H.E., Specht, E., Broedbaek, K., Henriksen, T., Ellervik, C., Mandrup-Poulsen, T., Tonnesen, M., Nielsen, P.E., Andersen, H.U., and Weimann, A. (2012). RNA modifications by oxidation: a novel disease mechanism? Free Radic. Biol. Med. *52*, 1353–1361.
6. Li, Z., Wu, J., and Deleo, C.J. (2006). RNA damage and surveillance under oxidative stress. IUBMB Life *58*, 581–588.
7. Li, Z., Malla, S., Shin, B., and Li, J.M. (2014). Battle against RNA Oxidation: Molecular Mechanisms for Reducing Oxidized RNA to Protect Cells, *5* (Wiley Interdiscip Rev RNA), pp. 335–346.
8. Broedbaek, K., Siersma, V., Henriksen, T., Weimann, A., Petersen, M., Andersen, J.T., Jimenez-Solem, E., Stovgaard, E.S., Hansen, L.J., Henriksen, J.E., et al. (2011). Urinary markers of nucleic acid oxidation and long-term mortality of newly diagnosed type 2 diabetic patients. Diabetes Care *34*, 2594–2596.
9. Broedbaek, K., Siersma, V., Henriksen, T., Weimann, A., Petersen, M., Andersen, J.T., Jimenez-Solem, E., Hansen, L.J., Henriksen, J.E., Bonnema, S.J., et al. (2013). Association between urinary markers of nucleic acid oxidation and mortality in type 2 diabetes: a population-based cohort study. Diabetes Care *36*, 669–676.
10. Mao, Y.H., Xu, L.N., Weng, Q.H., Li, X.Y., Zhao, B., Nie, J.J., Hu, J.H., Zhang, L.Q., Chen, Z., Zuo, M.Z., et al. (2018). The Ratio of Plasma and Urinary 8-oxo-Gsn Could Be a Novel Evaluation Index for Patients with Chronic Kidney Disease. Oxid. Med. Cell. Longev. *2018*, 4237812.
11. Wang, W.X., Luo, S.B., Jiang, P., Xia, M.M., Hei, A.L., Mao, Y.H., Li, C.B., Hu, G.X., and Cai, J.P. (2017). Increased Oxidative Damage of RNA in EarcrossStage Nephropathy in db/db Mice. Oxid. Med. Cell. Longev. *2017*, 2353729.
12. Wurtmann, E.J., and Wolin, S.L. (2009). RNA under attack: cellular handling of RNA damage. Crit. Rev. Biochem. Mol. Biol. *44*, 34–49.
13. Chanfreau, G.F. (2017). Impact of RNA Modifications and RNA-Modifying Enzymes on Eukaryotic Ribonucleases. Enzymes *41*, 299–329.
14. Dos Santos, R.F., Quendera, A.P., Boavida, S., Seixas, A.F., Arraiano, C.M., and Andrade, J.M. (2018). Major 3'-5' Exoribonucleases in the Metabolism of Coding and Non-coding RNA. Prog. Mol. Biol. Transl. Sci. *159*, 101–155.
15. Nguyen, L.H., Espert, L., Mechti, N., and Wilson, D.M., 3rd (2001). The human interferon- and estrogen-regulated ISG20/HEM45 gene product degrades single-stranded RNA and DNA in vitro. Biochemistry *40*, 7174–7179.
16. Espert, L., Eldin, P., Gongora, C., Bayard, B., Harper, F., Chelbi-Alix, M.K., Bertrand, E., Degols, G., and Mechti, N. (2006). The exonuclease ISG20 mainly localizes in the nucleolus and the Cajal (Coiled) bodies and is associated with nuclear SMN protein-containing complexes. J. Cell. Biochem. *98*, 1320–1333.
17. Deymier, S., Louvat, C., Fiorini, F., and Cimarelli, A. (2022). ISG20: an enigmatic antiviral RNase targeting multiple viruses. FEBS Open Bio *12*, 1096–1111.
18. Vascotto, C., Fantini, D., Romanello, M., Cesaratto, L., Deganuto, M., Leonardi, A., Radicella, J.P., Kelley, M.R., D'Ambrosio, C., Scaloni, A., et al. (2009). APE1/Ref-1 interacts with NPM1 within nucleoli and plays a role in the rRNA quality control process. Mol. Cell. Biol. *29*, 1834–1854.
19. Wu, J., and Li, Z. (2008). Human polynucleotide phosphorylase reduces oxidative RNA damage and protects HeLa cell against oxidative stress. Biochem. Biophys. Res. Commun. *372*, 288–292.
20. Piwowarski, J., Grzechnik, P., Dziembowski, A., Dmochowska, A., Minczuk, M., and Stepien, P.P. (2003). Human polynucleotide phosphorylase, hPNPase, is localized in mitochondria. J. Mol. Biol. *329*, 853–857.
21. Whitaker, A.M., and Freudenthal, B.D. (2018). APE1: A skilled nucleic acid surgeon. DNA repair *71*, 93–100.
22. Chohan, M., Mackedenski, S., Li, W.M., and Lee, C.H. (2015). Human apurinic/apyrimidinic endonuclease 1 (APE1) has 3' RNA phosphatase and 3' exoribonuclease activities. J. Mol. Biol. *427*, 298–311.
23. Shan, X., Chang, Y., and Lin, C.l.G. (2007). Messenger RNA oxidation is an early event preceding cell death and causes reduced protein expression. FASEB J. *21*, 2753–2764.
24. Tanaka, M., and Chock, P.B. (2021). Oxidative Modifications of RNA and Its Potential Roles in Biosystem. Front. Mol. Biosci. *8*, 685331.
25. Nunomura, A., Perry, G., Pappolla, M.A., Wade, R., Hirai, K., Chiba, S., and Smith, M.A. (1999). RNA oxidation is a prominent feature of vulnerable neurons in Alzheimer's disease. J. Neurosci. *19*, 1959–1964.
26. Honda, K., Smith, M.A., Zhu, X., Baus, D., Merrick, W.C., Tartakoff, A.M., Hattier, T., Harris, P.L., Siedlak, S.L., Fujioka, H., et al. (2005). Ribosomal RNA in Alzheimer disease is oxidized by bound redox-active iron. J. Biol. Chem. *280*, 20978–20986.
27. Karagöz, G.E., Acosta-Alvear, D., and Walter, P. (2019). The Unfolded Protein Response: Detecting and Responding to Fluctuations in the Protein-Folding Capacity of the Endoplasmic Reticulum. Cold Spring Harb. Perspect. Biol. *11*, a033886.
28. Fribley, A., Zhang, K., and Kaufman, R.J. (2009). Regulation of apoptosis by the unfolded protein response. Methods Mol. Biol. *559*, 191–204.
29. Walter, P., and Ron, D. (2011). The unfolded protein response: from stress pathway to homeostatic regulation. Science *334*, 1081–1086.
30. Hetz, C. (2012). The unfolded protein response: controlling cell fate decisions under ER stress and beyond. Nat. Rev. Mol. Cell Biol. *13*, 89–102.
31. Yan, M., Shu, S., Guo, C., Tang, C., and Dong, Z. (2018). Endoplasmic reticulum stress in ischemic and nephrotoxic acute kidney injury. Ann. Med. *50*, 381–390.
32. Song, R., Gao, Y., Dozmorov, I., Malladi, V., Saha, I., McDaniel, M.M., Parameswaran, S., Liang, C., Arana, C., Zhang, B., et al. (2021). IRF1 governs the differential interferon-stimulated gene responses in human monocytes and macrophages by regulating chromatin accessibility. Cell Rep. *34*, 108891.
33. Gongora, C., Degols, G., Espert, L., Hua, T.D., and Mechti, N. (2000). A unique ISRE, in the TATA-less human Isg20 promoter, confers IRF-1-mediated responsiveness to both interferon type I and type II. Nucleic Acids Res. *28*, 2333–2341.
34. Wang, Y., John, R., Chen, J., Richardson, J.A., Shelton, J.M., Bennett, M., Zhou, X.J., Nagami, G.T., Zhang, Y., Wu, Q.Q., and Lu, C.Y. (2009). IRF-1 promotes inflammation early after ischemic acute kidney injury. J. Am. Soc. Nephrol. *20*, 1544–1555.
35. Hayakawa, H., Uchiumi, T., Fukuda, T., Ashizuka, M., Kohno, K., Kuwano, M., and Sekiguchi, M. (2002). Binding capacity of human YB-1 protein for RNA containing 8-oxoguanine. Biochemistry *41*, 12739–12744.
36. Hayakawa, H., Fujikane, A., Ito, R., Matsumoto, M., Nakayama, K.I., and Sekiguchi, M. (2010). Human proteins that specifically bind to 8-oxoguanine-containing RNA and their responses to oxidative stress. Biochem. Biophys. Res. Commun. *403*, 220–224.

37. Zhou, M., Tang, W., Fu, Y., Xu, X., Wang, Z., Lu, Y., Liu, F., Yang, X., Wei, X., Zhang, Y., et al. (2015). Progranulin protects against renal ischemia/reperfusion injury in mice. Kidney Int. *87*, 918–929.

38. Yuen, P.S.T., Dunn, S.R., Miyaji, T., Yasuda, H., Sharma, K., and Star, R.A. (2004). A simplified method for HPLC determination of creatinine in mouse serum. Am. J. Physiol. Ren. Physiol. *286*, F1116–F1119.

39. Fountain, K.J., Kloss, A., Garibyan, I., Blitshteyn, B., Brezzani, A., Kyostio-Moore, S., Zuk, A., Sacchiero, R., and Cohen, A.S. (2007). Analysis of creatinine in mouse and rat serum by ion exchange high performance liquid chromatography for in vivo studies of renal function. J. Chromatogr. B Analyt. Technol. Biomed. Life Sci. *846*, 245–251.

40. Liu, M., Liang, K., Zhen, J., Zhou, M., Wang, X., Wang, Z., Wei, X., Zhang, Y., Sun, Y., Zhou, Z., et al. (2017). Sirt6 deficiency exacerbates podocyte injury and proteinuria through targeting Notch signaling. Nat. Commun. *8*, 413.

41. Zhan, P., Zhang, Y., Shi, W., Liu, X., Qiao, Z., Wang, Z., Wang, X., Wu, J., Tang, W., Sun, Y., et al. (2022). Myeloid-derived growth factor deficiency exacerbates mitotic catastrophe of podocytes in glomerular disease. Kidney Int. *102*, 546–559.

42. Jing, X., Ren, D., Gao, F., Chen, Y., Wu, X., Han, Y., Han, Q., Li, L., Wang, X., Tang, W., and Zhang, Y. (2021). Gene deficiency or pharmacological inhibition of PDCD4-mediated FGR signaling protects against acute kidney injury. Acta Pharm. Sin. B *11*, 394–405.

43. Fang, W., Wang, Z., Li, Q., Wang, X., Zhang, Y., Sun, Y., Tang, W., Ma, C., Sun, J., Li, N., and Yi, F. (2018). Gpr97 Exacerbates AKI by Mediating Sema3A Signaling. J. Am. Soc. Nephrol. *29*, 1475–1489.

44. Fu, Y., Sun, Y., Wang, M., Hou, Y., Huang, W., Zhou, D., Wang, Z., Yang, S., Tang, W., Zhen, J., et al. (2020). Elevation of JAML Promotes Diabetic Kidney Disease by Modulating Podocyte Lipid Metabolism. Cell Metab. *32*, 1052–1062.e8.

45. Kim, M., Ham, A., Kim, J.Y., Brown, K.M., D'Agati, V.D., and Lee, H.T. (2013). The volatile anesthetic isoflurane induces ecto-5'-nucleotidase (CD73) to protect against renal ischemia and reperfusion injury. Kidney Int. *84*, 90–103.

46. Dai, D.P., Gan, W., Hayakawa, H., Zhu, J.L., Zhang, X.Q., Hu, G.X., Xu, T., Jiang, Z.L., Zhang, L.Q., Hu, X.D., et al. (2018). Transcriptional mutagenesis mediated by 8-oxoG induces translational errors in mammalian cells. Proc. Natl. Acad. Sci. USA. *115*, 4218–4222.